

# Frequency adjustable Resonator as a Tunable Coupler for Xmon Qubits

Hui Wang,<sup>1,2</sup> Yan-Jun Zhao,<sup>3,\*</sup> Rui Wang,<sup>4,5</sup> Xun-Wei Xu,<sup>6</sup> Qiang Liu,<sup>1,7</sup> Jianhua Wang,<sup>1</sup> and Changxin Jin<sup>1</sup>

<sup>1</sup>*Inspur Academy of science and technology, Jinan, China*

<sup>2</sup>*Inspur artificial intelligence research institute, Jinan, China*

<sup>3</sup>*Key Laboratory of Opto-electronic Technology, Ministry of Education,  
Beijing University of Technology, Beijing, China*

<sup>4</sup>*Department of Physics, Tokyo University of Science,  
1-3 Kagurazaka, Shinjuku, Tokyo 162-0825, Japan.*

<sup>5</sup>*RIKEN Center for Quantum Computing (RQC), Wako, Saitama 351-0198, Japan*

<sup>6</sup>*Key Laboratory of Low-Dimensional Quantum Structures and Quantum Control of Ministry of Education,  
Key Laboratory for Matter Microstructure and Function of Hunan Province,  
Department of Physics and Synergetic Innovation Center for Quantum Effects and Applications,  
Hunan Normal University, Changsha 410081, China*

<sup>7</sup>*Inspur artificial intelligence research institute quantum computer*

(Dated: August 22, 2022)

We propose a scheme of tunable coupler based on a frequency adjustable resonator for scalable quantum integrated circuits. One side of the T-shape quarter-wave resonator is short to the ground through a DC SQUID, which is used to tune the frequency of the resonator coupler. In the other side with two open ends, either end capacitively couples to a different Xmon qubit, which determines the effective coupling between the two qubits. The fundamental mode of the tunable resonator dominates the interaction with the qubits and functions as a tunable coupler to switch off/on the qubit-qubit interaction. The required external magnetic flux for the tunable coupler's switching off frequency is affected by the asymmetry degree of the DC SQUID, which can help to choose a better noise environment (of the qubits) induced by the resonator coupler. The T-shape tunable resonator can help to reduce the direct interaction between two qubits, which should be an important way to suppress the ZZ crosstalk and realize high-fidelity quantum gates. The DC SQUID is several millimeters away from the Xmon qubits, which in principle creates less flux noises compared with the transmon-type coupler.

## I. INTRODUCTION

High-quality two-qubit quantum gates are the key step for future large-scale superconducting quantum processor and quantum error correction. Dynamically tuning the qubit-qubit coupling greatly enhances the fidelity of two qubit quantum gate, and the schemes include the tunable inductance [1], transmon coupler[2, 3], rf-SQUID[4], resonator coupler[5–7], floating coupler[8], and so on. In the past few years, the high-precision control of multiple qubits on superconducting quantum chips have been experimentally realized[5, 6, 9–13]. But the residual ZZ crosstalk and state leakage still limit for further improvement on control precision for superconducting quantum processor. Many experimental schemes have been used to suppress the ZZ crosstalk and realize high-fidelity two-qubit quantum gates[1, 7, 8, 14–18].

The superconducting resonator is easy to fabricate and measure, which has been used as the coupler in the superconducting quantum processor. For example, IBM have developed the 'Eagle' quantum processor with to date the largest number of 127 transmon qubits[5, 6]. But in most experiments, the frequencies of resonator-type couplers are fixed, and the qubit-qubit interaction can not be totally switched off. By embedding a DC SQUID inside the superconducting resonator, some experiments have tuned resonator's frequency by more than 500 Megahertz, and the tuning speed can be faster than the lifetime of photons[19–24]. Recently the exponentially large on-off ratio has been realized in experiment with a nonlinear mode of resonator as the tunable superconducting coupler [25].

In this paper, we propose a theoretical scheme of using a T-shape quarter-wave resonator to dynamically tune the coupling between two Xmon qubits. The open ends of T-shape resonator capacitively couple to two qubits, while the other end is a DC SQUID which dominates the inductive energy of the resonator coupler. Considering the tunable frequency with the external magnetic flux and largely non-equidistant basic modes, the fundamental mode of quarter-wave resonator could function as a tunable coupler to switch off/on the qubit-qubit coupling. For the asymmetric DC SQUID, the required external magnetic flux for the fundamental mode to reach the switch off frequency can be farther

---

\* Correspondence:zhao'yanjun@bjut.edu.cn

from the half-integer quantum flux, and the degree of asymmetry could help to choose a better noise environment for the Xmon qubits. With the transversely broaden part of T-type resonator at the open to weaken the direct qubit-qubit coupling, the ZZ crosstalk can be suppressed to several kilohertz which guarantees the realizability of the high fidelity quantum gates. And the DC SQUID is almost 5 mm away and needs a small current to control the magnetic flux, so the resonator coupler should create less flux noises to Xmon qubits. Compared with the transmon type coupler, the resonator-based coupler is easily to fabricate and measure, and has the potential advantages of saving the dilution refrigerator lines.

The paper is organized as follows: In Sec. II, we discuss the theoretical model of a three-body system, In Sec. III, we analyze the cavity modes' frequencies and anharmonicities. In Sec. IV, we study the effective qubit-qubit coupling, ZZ crosstalk, and state leakage to the resonator coupler. We finally summarize the results in Sec. V.

## II. THE PHYSICAL MODEL

As shown in Fig. 1(a), we study a three-body system consisting of two qubits capacitively coupling to a common T-shape quarter-wave resonator, the DC SQUID is far away and does not participate in the interaction with qubits. Then the Hamiltonian of three-body system can be written as

$$H = \sum_{j=1}^2 \frac{\hbar}{2} \omega_j \sigma_j^z + \sum_n \hbar \omega_c^{(n)} (\Phi_{e,s}) a_n^\dagger a_n \quad (1)$$

$$+ \sum_{j,n} \frac{\hbar}{2} g_{jc}^{(n)} [\sigma_j^+ a_n + \sigma_j^- a_n^\dagger] + \hbar g_{12} [\sigma_1^- \sigma_2^+ + \sigma_2^- \sigma_1^+],$$

here  $\omega_j$  are the transition frequencies of qubits, where the subscript  $j = 1, 2$ . The symbols  $a_n^\dagger$  and  $a_n$  are the creation and annihilation operators of the  $n$ -th resonator mode's photons, while  $\sigma_j^\pm$  and  $\sigma_j^z$  are the ladder operators and Pauli Z operators of the two qubits, respectively. And  $\omega_c^{(n)}$  ( $n$  are integers) is the  $n$ -th mode of the T-shape quarter-wave resonator. As will be discussed in the following Sections, the inductive energy of DC SQUID is much larger than that of transmission line resonator, and the frequency of the quarter-wave resonator can be continually tuned by the external magnetic flux  $\Phi_{e,s}$ . The quantity  $g_{12}$  is the direct coupling strength between two qubits, and  $g_{jc}^{(n)}$  describe coupling strengths of qubits with  $n$ -th resonator mode. The qubit-resonator coupling strength  $g_{jc}^{(n)}$  also depends on external magnetic flux  $\Phi_{e,s}$  as will be discussed in the following Sections.

The switching off frequency for qubit-qubit coupling usually locates in the qubit-coupler large detuning regime, that is  $g_{jc}^{(n)} / |\Delta_j^{(n)}| \ll 1$ , where  $\Delta_j^{(n)} = \omega_j - \omega_c^{(n)}$ . Defining  $S = \sum_{j,n} (g_{jc}^{(n)} / \Delta_j^{(n)}) [a_n^\dagger \sigma_j^- - a_n \sigma_j^+]$ , under the unitary transformation  $H' = \exp(-S) H \exp(S)$ , then we get the effective Hamiltonian in the large detuning regime as

$$H' \approx \sum_n \hbar \left[ \omega_c^{(n)} + \sum_{j=1}^2 \frac{[g_{jc}^{(n)}]^2}{\Delta_j^{(n)}} \sigma_j^z \right] a_n^\dagger a_n$$

$$+ \frac{\hbar}{2} \sum_j \left[ \omega_j + \sum_{n=1}^2 \frac{[g_{jc}^{(n)}]^2}{\Delta_j^{(n)}} \right] \sigma_j^z$$

$$+ \hbar \left[ g_{12} + \sum_n \frac{g_{1c}^{(n)} g_{2c}^{(n)}}{\Delta_e^{(n)}} \right] [\sigma_1^- \sigma_2^+ + \sigma_2^- \sigma_1^+]. \quad (2)$$

Here,  $2/\Delta_e^{(n)} = 1/\Delta_1^{(n)} + 1/\Delta_2^{(n)}$ , and the condition  $g_{12} \ll g_{jc}^{(n)} \ll |\Delta_j^{(n)}|$  has been used above. The representation  $(g_{1c}^{(n)} g_{2c}^{(n)})/\Delta_e^{(n)}$  describes the amplitude of indirect qubit-qubit coupling induced by the  $n$ -th resonator mode, and the qubit-qubit coupling is switched off when  $\sum_n g_{1c}^{(n)} g_{2c}^{(n)} / \Delta_e^{(n)} = -g_{12}$ , here  $n$  is an integer.

As will be discussed in the following Sections, the spectrum anharmonicities of T-shape quarter-wave resonator are very large and can reach Gigahertz, so the modes hybridization induced by qubits could be neglected. So the fundamental mode of the tunable resonator will dominate the interactions with the qubits and functions as a tunable coupler for the superconducting qubits. If the frequency  $\omega_c^{(1)}(\Phi_{e,s})$  is tuned to a certain frequency to satisfy  $g_{1c}^{(1)} g_{2c}^{(1)} / \Delta_e^{(1)} = -g_{12}$ , then the qubit-qubit coupling can be totally switched off for an isolated single-qubit quantum gate. Moving away from this frequency, the qubit-qubit coupling will be switched on to allow the multi-qubit quantum gates.

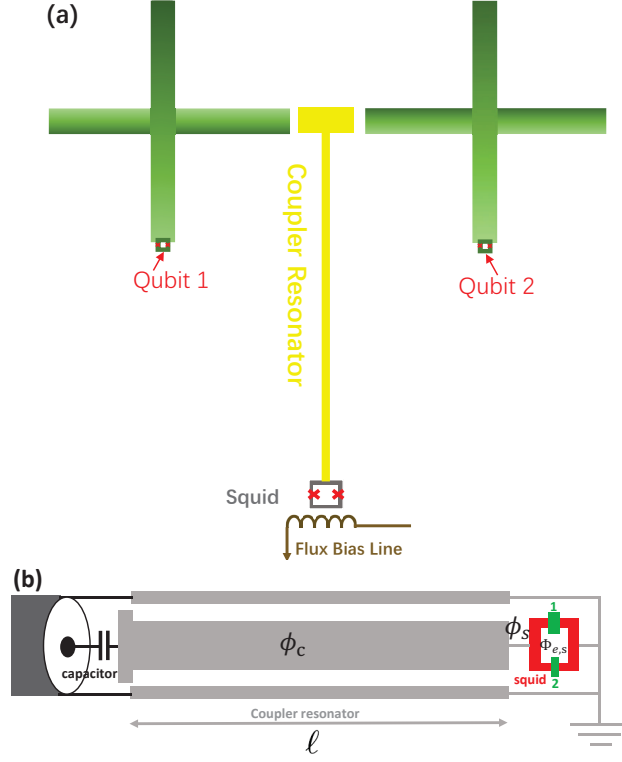


FIG. 1. (Color online) T-type quarter-wave resonator functioning as the tunable coupler for two Xmon qubits. (a) Diagram sketch of the three-body system. One side of the resonator with the two ends capacitively couples to two different qubits, and the other side is short to the ground through a DC SQUID. The transverse width of T-shape resonator is much smaller than the longitudinal length ( $\ell$ ). (b) Detailed sketch of the T-shape quarter-wave resonator[24]. Here  $\phi_c$  is the superconducting phase of resonator, while  $\phi_s$  is the boundary value of the cavity field at the SQUID, and the external magnetic flux  $\Phi_{e,s}$  could tune the frequency of the resonator coupler.

### III. T-SHAPE QUARTER-WAVE RESONATOR

Figure 1(a) describes a three-body system consisting of two Xmon qubits and a T-shape quarter-wave resonator, the fundamental mode of the resonator functions as a tunable coupler for the qubit-qubit coupling. The detailed sketch of tunable resonator is shown in Fig. 1(b), it is a deformed quarter-wave resonator with a transversely broadened part at the open end (left side), and the other end (right side) is short to the ground through a DC SQUID. The longitudinal length of transmission line resonator is  $\ell$  (about 4.87mm), which is much larger than the transverse width (usually below  $100\mu\text{m}$ ), so the effects of the transversely broadened part on resonator coupler's basic modes can be neglected.

The capacitance and inductance per unit length are  $C_0$  and  $L_0$ , respectively. The DC SQUID consists of two junctions with critical currents  $I_{cs_{1,2}}$ , respectively, and  $C_{s_{1,2}}$  are their capacitances. The quantities  $\phi_{s_{1,2}}$  are the superconducting phases across the junctions 1 and 2 of the DC SQUID, respectively, and they satisfy the relation  $\phi_{s_1} - \phi_{s_2} = 2\pi n + 2\pi\Phi_{e,s}/\Phi_0$  ( $n$  is an integer). Then the Lagrangian of the T-shape quarter-wave resonator is

$$\begin{aligned}
 L_{qwr} = & \left(\frac{\Phi_0}{2\pi}\right)^2 \int_0^\ell \left[ \frac{C_0}{2} \dot{\phi}_c^2(x, t) - \frac{[\partial_x \phi_c(x, t)]^2}{2L_0} \right] dx \\
 & + \frac{\hbar^2}{8E_{C_{s_1}}} \dot{\phi}_{s_1}^2 + E_{Js_1} \cos(\phi_{s_1}) \\
 & + \frac{\hbar^2}{8E_{C_{s_2}}} \dot{\phi}_{s_2}^2 + E_{Js_2} \cos(\phi_{s_2}).
 \end{aligned} \tag{3}$$

Here  $E_{Cs_{1,2}} = e^2/(2C_{s_{1,2}})$  and  $E_{Js_{1,2}} = -\Phi_0 I_{cs_{1,2}}/(2\pi)$  describe the charging energies and Josephson energies of SQUID's two junctions, respectively. Here  $\phi_c(x, t)$  is the superconducting phase operator of the resonator, and  $\Phi_0 = h/2e$  is the flux quantum. If we define  $E_{Jt} = E_{Js_1} + E_{Js_2}$ , then the effective Josephson energy of the DC

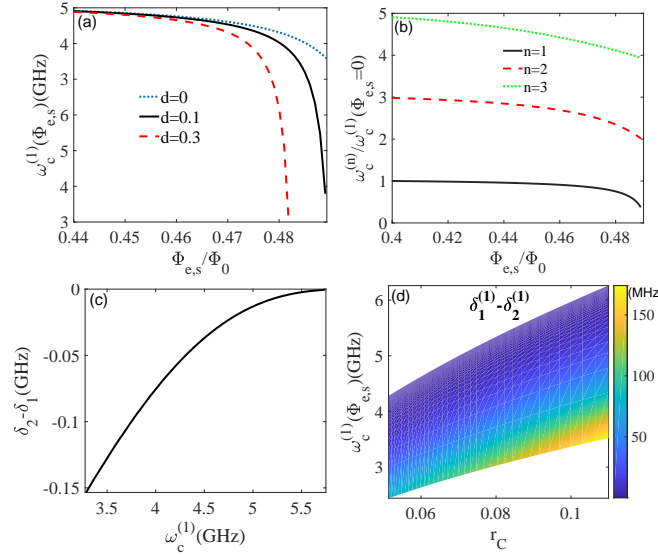


FIG. 2. (Color online) Frequencies and anharmonicities for the tunable resonator's basic modes. (a) Fundamental mode's frequencies  $\omega_c^{(1)}$  changing with the external magnetic flux  $\Phi_{e,s}$  under different asymmetries  $d$  of the SQUID; (b) three lowest basic modes' frequencies  $\omega_c^{(n)}$  ( $n = 1, 2, 3$ ) changing with the magnetic flux  $\Phi_{e,s}$ ; (c) anharmonicity  $(\delta_2^{(1)} - \delta_1^{(1)})$  of fundamental mode's two lowest energy levels changing with  $\omega_c^{(1)}$ ; (d) anharmonicity  $(\delta_2^{(1)} - \delta_1^{(1)})$  changing with the frequency  $\omega_c^{(1)}$  and the capacitance  $(C_0\ell)$ , with  $r_C = C_s/C_0\ell$ . The longitudinal length of resonator coupler  $\ell = 4.87$  mm, the capacitance per unit length  $C_0 = 0.16$  nF/m [except in (d)] and inductance per unit length  $L_0 = 0.44$   $\mu$ H/m. The other parameters are:  $r_L = 0.02$ ,  $r_C = 0.1$ ,  $d = 0.1$  [except in (a)], the SQUID's inductance  $C_s = 75$  fF, and the fundamental mode's frequency of the bare resonator is  $\omega_c^{(b)}(\Phi_{e,s} = 0) = 6$  GHz [except in (d)].

SQUID can be obtained as  $E_{Js} = E_{Jt} \sqrt{\cos(\pi\Phi_{e,s}/\Phi_0)^2 + d^2 \sin^2(\pi\Phi_{e,s}/\Phi_0)}$ , where  $d = (E_{Js1} - E_{Js2})/(E_{Js1} + E_{Js2})$  describes the junction asymmetry[26]. The DC SQUID can be regarded as an inductor with the tunable inductance,

$$L_{sq} = \frac{\Phi_0/(2\pi I_{cs})}{\sqrt{\cos^2\left(\frac{\pi\Phi_{e,s}}{\Phi_0}\right) + d^2 \sin^2\left(\frac{\pi\Phi_{e,s}}{\Phi_0}\right) \cos(\phi_s - \phi_0)}}, \quad (4)$$

here  $I_{cs} = I_{cs1} + I_{cs2}$  is the sum of the critical currents of the two junctions, and the phase  $\phi_0$  can be solved from the equation:  $\tan \phi_0 = d \tan(\pi\Phi_{e,s}/\Phi_0)$ . The boundary value of cavity field at the SQUID is defined as  $\phi_s = (\phi_{s1} + \phi_{s2})/2$  which can be considered as the resonator's superconducting phase at the SQUID. For typical dimensions of devices, the Josephson energy of the DC SQUID is much larger than that of transmission line resonator and dominates the inductive energy of the resonator coupler, so the frequency of the resonator coupler can be tuned by external magnetic flux  $\Phi_{e,s}$  passing through the SQUID loop. Some experiments have realized fast tuning of resonator frequency exceeding 500 Megahertz and even one Gigahertz[19–21].

The resonator's superconducting phase field  $\phi_c$  follows the wave equation  $\ddot{\phi}_c - v^2 \phi_c'' = 0$ , which can be expanded with the resonator's eigen-modes, then yielding  $\phi_c(x, t) = (2e/\hbar) \sqrt{(2/C_c\ell)} \sum_n q_n(t) \cos(k_n x)$  ( $n$  are integers). Here  $\omega_c^{(n)}$  is the frequency of  $n$ -th basic mode,  $q_n(t)$  are time-dependent coefficients and  $k_n = \omega_c^{(n)}/v$ , and  $v = 1/\sqrt{L_0 C_0}$  is the phase velocity. At the open end  $\partial_x \phi_c(x, t)|_{x=0} = 0$ , while the boundary value of cavity field at the SQUID satisfies  $\phi_s(x, t) = \phi_c(x, t)|_{x=\ell}$ , the motion equation of  $\phi_s$  can be written as  $\hbar^2 \ddot{\phi}_s / E_{Cs} + 2E_{Js} \cos(\pi\Phi_{e,s}/\Phi_0) \sin(\phi_s) + \ell E_{L,cav} \phi_s' = 0$ , where  $\phi_s' = \partial_x \phi_s(x, t)$ , and  $E_{L,cav} = (\hbar/2e)^2 / (L_0 \ell)$  is the inductive energy of transmission line resonator[22–24]. In this paper we focus on the regime  $|\phi_s| \ll 1$ , and the  $\phi_s$  decouples from other variables of quarter-wave resonator. Under the static bias current, the superconducting phase field can be formally written as  $\phi_c(x, t) \propto \cos(k_n x) \exp(\pm i\omega_n t)$ . Substituting it into the motion equation of  $\phi_s$ , gives the dispersion relation for the  $n$ -th mode, i.e.,

$$0 = k_n \ell \tan(k_n \ell) + r_C (k_n \ell)^2 - \frac{\cos(\phi_s - \phi_0)}{r_L} \times \sqrt{\cos^2\left(\frac{\pi\Phi_{e,s}}{\Phi_0}\right) + d^2 \sin^2\left(\frac{\pi\Phi_{e,s}}{\Phi_0}\right)}. \quad (5)$$

Here,  $r_C = C_s/C_0\ell$  is the capacitance ratio between the DC SQUID and the transmission line resonator, and  $r_L = E_{L,cav}/E_{J_s}$  is the ratio of inductive energies between the transmission line resonator and the DC SQUID. In this paper we focus on the regime  $E_{L,cav}/[2E_{J_s}^{(m)} \cos(\pi\Phi_{e,s}/\Phi_0)] \ll 1$  and  $|\phi_s| \ll 1$ , which guarantee the SQUID's variables decoupling from the resonator modes, here  $E_{J_s}^{(m)} = -\Phi_0 I_{cs}/(2\pi)$  maximal Josephson energy of DC SQUID. The numerical simulation results from Eq. (5) can be seen in Fig. 2. The blue-dotted curve in Fig. 2(a) describes the variations of the fundamental mode's frequency of symmetric DC SQUID ( $d = 0$ ), and the frequency of fundamental mode can be effectively tuned by the external magnetic flux. For the asymmetric DC SQUID, the fundamental mode's frequencies drop faster in the black-solid and red-dashed curves. This mainly originates from the dependence of  $\phi_0$  on flux  $\Phi_{e,s}$  ( $\phi_0 = 0$  for the symmetric DC SQUID), because the effects of  $\phi_s$  on the resonator modes' frequencies are very small in the case of  $|\phi_s| \ll 1$ . The basics modes' frequencies are shown in Fig. 2(b), so the effects of high-order modes can be neglected because of the large spectrum anharmonicities, and the fundamental mode dominates the interaction with qubits and functions as a tunable coupler for Xmon qubits.

Since  $r_L, r_C \ll 1$ , the second term in the right side of Eq. (5) contributes very little to the low-order modes, so the value of  $k_0\ell$  should be close to  $\pi/2$ . Next, we get an approximately analytical result for the fundamental mode's frequency,

$$\omega_c^{(1)} \approx \frac{\omega_c^{(b)}}{1 + \frac{r_L}{2\sqrt{\cos^2\left(\frac{\pi\Phi_{e,s}}{\Phi_0}\right) + d^2 \sin^2\left(\frac{\pi\Phi_{e,s}}{\Phi_0}\right)} \cos(\phi_s - \phi_0)}}, \quad (6)$$

where  $\omega_c^{(b)}$  describes the fundamental mode' frequency of the bare resonator ( $\Phi_{e,s} = 0$ ). Since  $\tan(k_n\ell/2)$  is a  $\pi$ -periodic function, the  $n$ -th resonator modes can be approximately written as  $\omega_c^{(n)} = \omega_c^{(1)} + n\pi/\ell$ . The dispersion relation of the resonator coupler under the linear approximations is shown in Eqs. (5) and (6). After adding the nonlinear corrections induced by the SQUID, the shift of  $m$ -th energy level for  $n$ -th basic mode can be obtained as  $\delta_m^{(n)} = -(6m^2 + 6m + 3)\lambda_n E_{L,cav}(m, n \text{ are integers})$ , with  $\lambda_n = \cos(k_n\ell)^2/[4(1 + 2k_n\ell/\sin(2k_n\ell))][27]$ . As shown in Fig. 2(c), the anharmonicity ( $\delta_2^{(1)} - \delta_1^{(1)}$ ) for two lowest energy levels of fundamental mode decreases when the magnetic flux passing through the SQUID loop departs from half-integer flux quantum. According to the simulation result in Fig. 2(d), an easy way of enhancing the fundamental mode's nonlinearity or anharmonicity is to reduce the transmission line resonator's capacitance.

Since the frequency tuning range for the resonator coupler is about several hundred Megahertz, to switch off qubit-qubit coupling in the qubit-resonator large detuning regime, the frequency of bare resonator should be very important and it is determined by the longitudinal length of resonator coupler. To effectively tune the frequency of the resonator coupler, the inductive energy of the DC SQUID should be much larger than that of the transmission line resonator, so the large critical current Josephson junctions of the DC SQUID are needed. The transmission line resonator's inductance and capacitance per unit length are obtained from the experiment result [24]. For the resonator coupler fabricated with a Niobium resonator and Aluminium SQUID, the detail parameters are: length  $\ell = 4.87$  mm, inductance per unit length  $0.44 \mu\text{H/m}$  and capacitance per unit length  $0.16 \text{ nF/m}$ , the inductive energy of transmission line resonator  $E_{L,cav}/\hbar = [\hbar/(2e)^2]/(L_0\ell) \approx 500 \text{ GHz}$ . The critical current of the DC SQUID should be around  $7.67 \mu\text{A}$  (for  $r_L = 0.02$ ), then the SQUID's maximal Josephson energy is  $E_{J_s}^{(m)}/\hbar = -\Phi_0 I_{cs}/(2\pi\hbar) \approx 2.4 \times 10^4 \text{ GHz}$ . Then the ratio of inductive energies for resonator and DC SQUID is  $E_{L,cav}/E_{J_s}^{(m)} \approx 1/100$ . For the resonator coupler with above parameters should be easy to fabricate with current nano-fabrication techniques. Similar to the transmon-type coupler, the quality factor of the resonator coupler will drop when an extra magnetic flux is applied to switch off/on qubit-qubit interaction[19]. The resonator coupler with low quality factor will induce dephasing of qubits, so it is important for the bare resonator to possess a relative high quality factor and the external magnetic flux to be farther from the half-integer quantum flux.

## IV. TUNABLE RESONATOR COUPLER

### A. Tunable Qubit-Qubit coupling

Circuit diagram for the three-body system is shown in Fig. 3(a), the capacitive coupling between any two of qubit 1, qubit 2, and resonator coupler depend on their frequencies and relative capacitances. In convenience, here and afterwards we regard the T-shape quarter-wave resonator as a lumped-element model. The fundamental mode of resonator functions as a tunable coupler for the Xmon qubits, and its frequency, inductance, and capacitance are  $\omega_c^{(1)}(\Phi_{e,s})$ ,  $L_c(\Phi_{e,s})$ , and  $C_c$ , respectively. Besides,  $C_j$ ,  $L_j$ ,  $\omega_j$  ( $j = 1, 2$ ) are the capacitances, inductances and

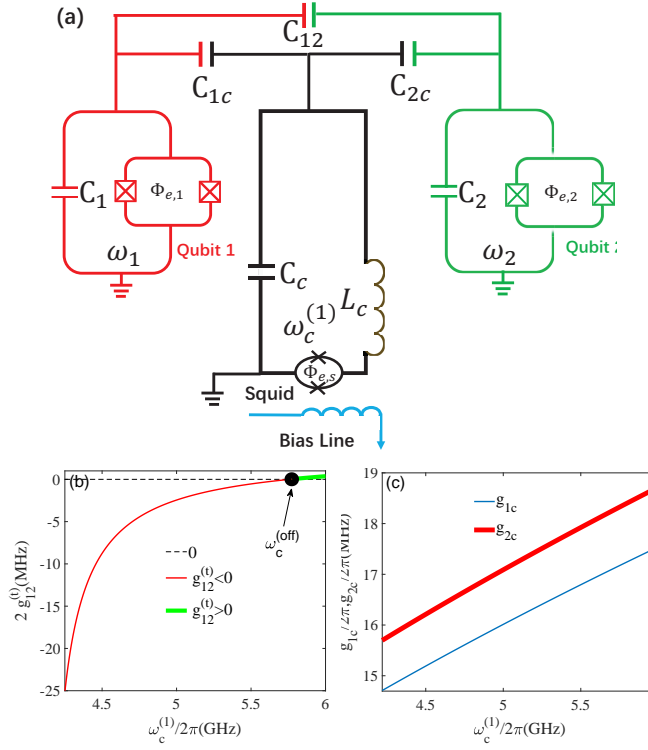


FIG. 3. (Color online) Switching off/on the qubit-qubit coupling with the resonator coupler. (a) Circuit Diagram of the three-body system.  $C_j$ ,  $L_j$ ,  $\omega_j$ , and  $\Phi_{e,j}$  ( $j = 1, 2, c$ ) are the capacitances, inductances, frequencies, and magnetic fluxes of Xmon qubits and resonator coupler, respectively. The quantity  $C_{12}$  is the capacitance between two Xmon qubits,  $C_{1c}$  and  $C_{2c}$  are relative capacitances of qubits 1 and 2 to resonator coupler, respectively. The coupling strengths of (b) qubit-qubit  $g_{12}^{(t)}$  and (c) qubit-resonator  $g_{jc}^{(1)}$  ( $j = 1, 2$ ) changing with the fundamental mode's frequency  $\omega_c^{(1)}$ . The other parameters are:  $\omega_1/(2\pi) = 4.0$  GHz,  $\omega_2/(2\pi) = 4.1$  GHz,  $r_L = 0.02$ ,  $r_C = 0.1$ ,  $d = 0.1$ ,  $g_{12}/(2\pi) = 1.3$  MHz,  $C_c = 0.78$  pF,  $C_1 = 100$  fF,  $C_2 = 90$  fF,  $C_{12} = 0.06$  fF,  $C_{1c} = 1$  fF, and  $C_{2c} = 1$  fF.

transition frequencies of qubits 1 and 2, respectively. Additionally,  $C_{12}$  is the relative capacitance between two qubits, and  $C_{jc}$  are the capacitances of qubits 1 and 2 relative to the resonator coupler, respectively. If the direct effects of the DC SQUID on the Xmon qubits are neglected, the kinetic (charging) energy of the system can be written as  $T = \sum_{j=1,2} [(C_j/2)\dot{\phi}_j^2 + (C_{jc}/2)(\dot{\phi}_j - \dot{\phi}_c)^2] + (C_c/2)\dot{\phi}_c^2 + (C_{12}/2)(\dot{\phi}_1 - \dot{\phi}_2)^2 + \sum_{k=1,2} (C_{sk}/2)\dot{\phi}_{sk}^2$ , and the potential (inductive) energy  $U = -\sum_{j=1,2} E_{J_j} \cos(\phi_j) + E_{L,cav}(\phi_c)^2 + E_{J_s} \cos(\phi_s - \phi_0)$ . The Lagrangian of the system can be obtained by  $L = T - U$ , after introducing  $q_j = \partial L / \partial \dot{\phi}_j$  ( $j = 1, 2, c$ ), the Hamiltonian of three-body system can be written as  $H_{ic} = \sum_{j=1,2,c} q_j \phi_j - L$ . Expressed with device's parameters, we get

$$\begin{aligned}
 H_{ic} = & \sum_{j=1}^2 [4E_{C_j}(N_j)^2 - E_{J_j} \cos(\phi_j)] \\
 & + 4E_{C_c}(N_c)^2 + E_{L,cav}(\phi_c)^2 \\
 & + 4E_{C_s}(N_s)^2 - E_{J_s} \cos(\phi_s - \phi_0) \\
 & + \sum_{j=1}^2 \left[ \frac{8C_{jc}}{\sqrt{C_j C_c}} \sqrt{E_{C_j} E_{C_c}} (N_j N_c) \right] \\
 & + 8 \left( 1 + \frac{C_{1c} C_{2c}}{C_{12} C_c} \right) \frac{C_{12}}{\sqrt{C_1 C_2}} \sqrt{E_{C_1} E_{C_2}} (N_1 N_2).
 \end{aligned} \tag{7}$$

The condition  $C_c \gg C_1, C_2 \gg C_{1c}, C_{1c} \gg C_{12}$  have been used. Here  $N_j$  are the number operators for charge quantization of Xmon qubits, and  $\phi_j$  are the phase operators, where the subscripts  $j = 1, 2$ . Their charging and Josephson energies are  $E_{C_j} = e^2/2C_j$  and  $E_{J_j} = -\Phi_0 I_{c_j}/2\pi$ , respectively, and  $I_{c_j}$  are the critical currents. For Xmon qubits,  $E_{J_j}/E_{C_j} \gg 1$ , then we can approximately obtain  $-E_{J_j} \cos(\phi_j) \approx -E_{J_j} + (E_{J_j}/2)\phi_j^2 - (E_{J_j}/24)\phi_j^4 + \dots$ ,



where the subscripts  $j = 1, 2$ . If we define  $\phi_j = (2E_{C_j}/E_{J_j})^{1/4}(c_j + c_j^\dagger)$  and  $N_j = i[E_{J_j}/(32E_{C_j})]^{1/4}(c_j - c_j^\dagger)$ , and the Hamiltonian of Xmon qubit can be written as  $H_{q_j} = \sqrt{8E_{C_j}E_{J_j}}(c_j^\dagger c_j + 1/2) - (E_{C_j}/12)(c_j^\dagger + c_j)^4 - E_{J_j}$ , and  $c_j^\dagger(c_j)$  are the creation (annihilation) operators of excited modes, where the subscripts  $j = 1, 2$ . The Xmon qubit's lowest transition energy level is  $\omega_j = (\sqrt{8E_{C_j}E_{J_j}} - E_{C_j})/\hbar$ , with the strength of anharmonicities  $\alpha_j = -E_{C_j}/\hbar$ .

For the resonator coupler,  $\phi_{c,s}$  are the superconducting phase operators of transmission line resonator and DC SQUID, respectively, while  $N_{c,s}$  are their charge number operators. The  $E_{C_s} = e^2/2(C_{s_1} + C_{s_2})$  and  $E_{J_s}$  are the total charging energy and Josephson energy of the DC SQUID, respectively. The inductive energy of the DC SQUID is much larger than that of the transmission line resonator, while the relation for charging energies is on the contrary, so the fundamental mode's frequency is determined by the inductive energy of the DC SQUID and charge energy of the transmission line resonator. The creation and annihilation operators of photons of the coupler resonator can be introduced by  $N_c = i[E_{J_s}/(32E_{C_c})]^{1/4}(a_1 - a_1^\dagger)$  and  $\phi_c = (2E_{C_c}/E_{J_s})^{1/4}(a_1 + a_1^\dagger)$ , and the frequency of fundamental mode for bare resonator ( $\Phi_{e,s} = 0$ ) is  $\omega_c^{(b)} = \sqrt{8E_{C_c}E_{J_s}}/\hbar$ . If an external magnetic flux is applied, the fundamental mode's frequency can be obtained by solving Eq. (5), then the effective Hamiltonian of tunable coupler becomes  $H_{tc} = \hbar(\omega_c^{(1)} + \delta_m^{(1)})a_1^\dagger a_1$ , while the  $\delta_m^{(1)}$  is the nonlinear energy level shift of  $m$ -photon state for the fundamental mode.

With the creation and annihilation operators, the Hamiltonian for the direct qubit-qubit interaction is  $H_{12} = -\hbar g_{12}(c_1 - c_1^\dagger)(c_2 - c_2^\dagger)$ , while the interaction Hamiltonians between the resonator coupler and qubits are  $H_{jc} = -\hbar g_{jc}^{(1)}(a_1 - a_1^\dagger)(c_j - c_j^\dagger)$ , where the subscripts  $j = 1, 2$ . Expressed with the device's parameters, then the direct qubit-qubit coupling strength becomes  $g_{12} = [(C_{12} + C_{1c}C_{2c}/C_c)/(2\sqrt{C_1C_2})]\sqrt{\omega_1\omega_2}$ , and the qubit-resonator coupling strengths are  $g_{jc}^{(1)} = [C_{jc}/(2\sqrt{C_jC_c})]\sqrt{\omega_j\omega_c^{(1)}}$  which also depends on the coupler's frequency  $\omega_c^{(1)}$  as shown in Fig. 3(c). To see clearer the indirect qubit-qubit interaction induced by the resonator coupler, we apply the Schrieffer-Wolf transformation, that is,  $U = \exp\{\sum_{j=1,2}[(g_{jc}^{(1)}/\Delta_j)(c_j^\dagger a_1 - c_j a_1^\dagger) - (g_{jc}^{(1)}/\Lambda_j)(c_j^\dagger a_1^\dagger - c_j a_1)]\}$ , with  $\Delta_j = \omega_j - \omega_c^{(1)}$  and  $\Lambda_j = \omega_j + \omega_c^{(1)}$  ( $j = 1, 2$ ). Then the resonator coupler is decoupled with Xmon qubits, and the decoupled Hamiltonian is  $H_d = \sum_{j=1,2}[\tilde{\omega}_j c_j^\dagger c_j + \frac{\tilde{\alpha}_j}{2} c_j^\dagger c_j^\dagger c_j c_j] + g_{12}^{(t)}(c_1^\dagger c_2 + c_1 c_2^\dagger)$ , where  $\tilde{\omega}_j \approx \omega_j + [g_{jc}^{(1)}]^2(1/\Delta_j - 1/\Lambda_j)$ ,  $\tilde{\alpha}_j \approx \alpha_j$ , where the subscripts  $j = 1, 2$ . The effective coupling strength between the two qubits is

$$g_{12}^{(t)} \approx \frac{1}{2} \left( 1 + \frac{C_{1c}C_{2c}}{C_c C_{12}} \right) \frac{C_{12}}{\sqrt{C_1C_2}} \sqrt{\omega_1\omega_2} + \frac{\omega_c^{(1)}}{8} \left[ \frac{1}{\Delta_1} + \frac{1}{\Delta_2} - \frac{1}{\Lambda_1} - \frac{1}{\Lambda_2} \right] \frac{C_{1c}C_{2c}}{C_c \sqrt{C_1C_2}} \sqrt{\omega_1\omega_2}. \quad (8)$$

The first line in Eq. (8) describes the direct capacitive qubit-qubit coupling, and the second line corresponds to the indirect qubit-qubit interaction induced by the resonator coupler. As shown in Fig. 2, the frequency  $\omega_c^{(1)}$  can be effectively tuned by the external magnetic flux, so the fundamental mode of T-shape quarter-wave resonator can function as a tunable coupler for Xmon qubits. The qubit-qubit coupling is totally switched off ( $g_{12}^{(t)} = 0$ ) at a certain frequency  $\omega_c^{(off)} = 4[1 + C_{12}C_c/(C_{1c}C_{2c})]/(1/\Lambda_1 + 1/\Lambda_2 - 1/\Delta_1 - 1/\Delta_2)$  as show in Fig. 3(b). As shown in Eq. (5), the indirect qubit-qubit coupling is proportional to the qubit-resonator coupling strength which is greatly affected by resonator coupler's parameters including the frequency  $\omega_c^{(1)}$  (see Fig. 3(c)), capacitance  $C_c$ , and the relative capacitances  $C_{jc}$ . And the direct qubit-qubit coupling is affected by relative capacitance between two qubits which can be weakened by enhancing the transverse broaden part of the resonator coupler in the open ends. So the T-shape quarter-wave resonator can help to realize a strong enough indirect coupling to switch off the qubit-qubit interaction and also a weak direct qubit-qubit interaction, which is an important way to suppress the ZZ crosstalk (as will be discussed in the following Sections).

## B. ZZ crosstalk

The Parasitic crosstalk between neighbour superconducting qubits is a leading limitation for quantum gates, and it is greatly affected by the anharmonicities of the qubits and resonator coupler. With the devices consisting of two couplers, some experiments finally cancel the qubit-qubit coupling and ZZ crosstalk[7, 17], but this will enhance complexities for the design, fabrication, and measurement processes, and some extra energy levels should be introduced. By assuming the opposite anharmonicities of two qubits, some research group proposed to totally cancel the ZZ crosstalk [14], but this should be very difficult in experiment. In this paper, we suppress the ZZ crosstalk by reducing the direct qubit-qubit coupling with the transversely broaden part of the T-shape quarter-wave resonator.

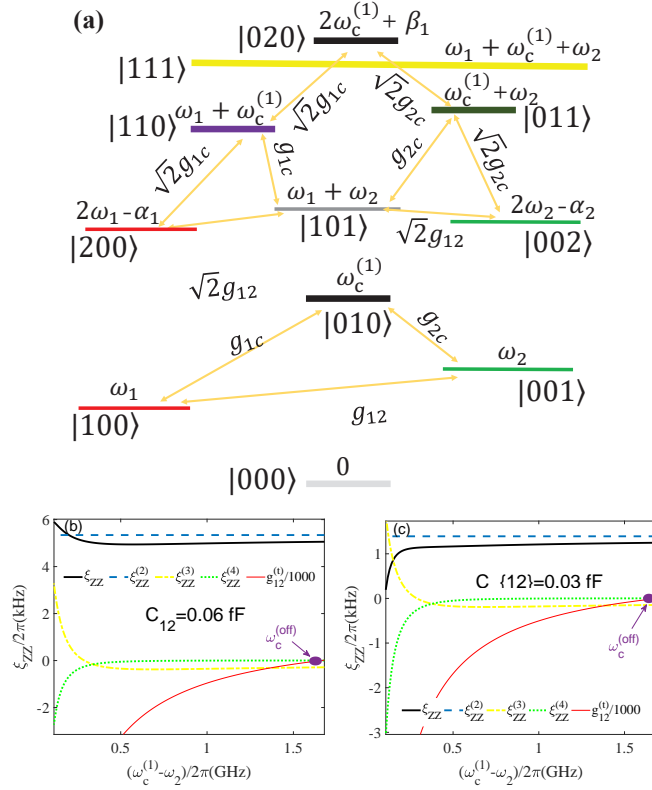


FIG. 4. (Color online) Residual ZZ crosstalk. (a) Energy level structure of the three-body system in the idle state. The ZZ crosstalk  $\xi_{ZZ}$  for the capacitance (b)  $C_{12} = 0.06$  fF and (c)  $C_{12} = 0.03$  fF. The parameters of the DC SQUID are the same as the black-solid curve in Fig. 2(a), while the parameters of the qubits and transmission line resonator are the same as in Fig. 3(b).

Figure 4(a) describes the energy level structure of the three-body system with qubits in the idle states, and the fundamental mode of resonator coupler is dispersive coupling with Xmon qubits. In the processes of two qubit quantum gates, some states will experience near resonant energy exchanges, such as  $|100\rangle \leftrightarrow |001\rangle$  and  $|101\rangle \leftrightarrow |200\rangle$  for the CZ (Controlled-Z) gates. According to the discussions in above Sections, after neglecting some virtual transition processes, the Hamiltonian of the three-body system becomes

$$\begin{aligned}
 H_{rwa} = & \hbar \left( \omega_c^{(1)} + \delta_m^{(1)} \right) a_1^\dagger a_1 \\
 & + \sum_{j=1}^2 \left[ \hbar \omega_j c_j^\dagger c_j + \frac{\hbar \alpha_j}{2} c_j^\dagger c_j^\dagger c_j c_j \right] \\
 & + \sum_{j=1}^2 \hbar g_{jc}^{(1)} \left( c_j a_1^\dagger + c_j^\dagger a_1 \right) + \hbar g_{12} \left( c_1 c_2^\dagger + c_1^\dagger c_2 \right),
 \end{aligned} \tag{9}$$

the rotating wave approximation has been used above. The  $\delta_m^{(1)}$  is the nonlinear energy level shift of the  $m$ -photon states for the resonator's fundamental mode, both  $\omega_c^{(1)}$  and  $\delta_m^{(1)}$  can be tuned by the external magnetic flux passing through the SQUID loop.

If the frequencies of qubits 1 and 2 are detuning, the residual ZZ crosstalk for the CZ gate can be defined as  $\xi_{ZZ} = \omega_{11} - \omega_{01} - \omega_{10}$  [3, 8, 16]. According to the numerical calculation in section III, we choose an anharmonicity value  $\delta_2^{(1)} - \delta_1^{(1)} = -50$  MHz for two lowest energy levels of the fundamental mode, the frequency  $\omega_c^{(1)}/2\pi$  is close to 4.5 GHz according to the curve in Fig. 2(c). The total ZZ crosstalk can be written as  $\xi_{ZZ} = \xi_{ZZ}^{(2)} + \xi_{ZZ}^{(3)} + \xi_{ZZ}^{(4)}$ , up to



fourth order small quantity [3, 16, 28, 29], we get

$$\xi_{ZZ}^{(2)} = \frac{2(g_{12})^2(\alpha_1 + \alpha_2)}{(\Delta_{12} + \alpha_1)(\Delta_{12} - \alpha_2)}, \quad (10)$$

$$\begin{aligned} \xi_{ZZ}^{(3)} = & 2g_{12}g_{1c}^{(1)}g_{2c}^{(1)} \left[ \frac{1}{\Delta_{1c}} \left( \frac{2}{\Delta_{12} - \alpha_2} - \frac{1}{\Delta_{12}} \right), \right. \\ & \left. - \frac{1}{\Delta_2} \left( \frac{2}{\Delta_{12} + \alpha_2} - \frac{1}{\Delta_{12}} \right) \right], \end{aligned} \quad (11)$$

$$\begin{aligned} \xi_{ZZ}^{(4)} = & \frac{2[g_{1c}^{(1)}g_{2c}^{(1)}]^2}{\Delta_1 + \Delta_2 + \delta_1^{(1)} - \delta_2^{(1)}} \left( \frac{1}{\Delta_{1c}} + \frac{1}{\Delta_{2c}} \right)^2 \\ & + \frac{[g_{1c}^{(1)}g_{2c}^{(1)}]^2}{\Delta_1^2} \left( \frac{2}{\Delta_{12} - \alpha_2} - \frac{1}{\Delta_{12}} - \frac{1}{\Delta_2} \right) \\ & - \frac{[g_{1c}^{(1)}g_{2c}^{(1)}]^2}{\Delta_{2c}^2} \left( \frac{2}{\Delta_{12} + \alpha_1} - \frac{1}{\Delta_{12}} + \frac{1}{\Delta_1} \right). \end{aligned} \quad (12)$$

Here  $\Delta_{12} = \omega_1 - \omega_2$  is the detuning between two qubits, and the  $\omega_1$  is fixed here. As shown in Figs. 4(b) and 4(c),  $|\xi_{ZZ}^{(2)}| \gg |\xi_{ZZ}^{(3)}| \gg |\xi_{ZZ}^{(4)}|$ , the second order term  $\xi_{ZZ}^{(2)}$  dominates the ZZ crosstalk in the qubit-resonator dispersive regime,[3, 17, 29]. The black-solid curve in Fig. 4(b) shows that the total ZZ crosstalk is in the magnitude order of several kilohertz, which is possible for realizing high fidelity quantum gates.

The  $\xi_{ZZ}^{(2)}$  in Eq.(10) is proportional to the square of direct qubit-qubit coupling ( $g_{12}^2$ ) and the total anharmonicity ( $\eta_1 + \eta_2$ ) of two Xmon qubits, while the third-order term  $\xi_{ZZ}^{(3)}$  in Eq.(11) and fourth-order term  $\xi_{ZZ}^{(4)}$  in Eq.(12) mainly depend on the qubit-resonator coupling strengths  $g_{jc}^{(1)}$ , where the subscripts  $j = 1, 2$ . If we increase the separation between two Xmon qubits with the help of the T-shape resonator coupler, then the relative capacitance  $C_{12}$  and direct qubit-qubit coupling strength  $g_{12}$  become smaller, then the ZZ crosstalk can be effectively suppressed as shown in Fig. 4(c).

### C. States leakages

In this paper, the switching off frequency for qubit-qubit coupling lies in the strong dispersive regime. Then the weak negative anharmonicity of the fundamental mode [see Fig. 2(c)] should push the state  $|020\rangle$  farther from the computational states, and this might reduce the leakage probability to the resonator coupler's double-photon states. The anharmonicity of the Xmon qubit is about several hundred Megahertz, which is much larger than qubit-resonator coupling strength. By introducing the bright and dark modes, the dynamic evolution in the CZ gate can be described by the following Hamiltonian[1, 16]

$$H_{|100\rangle \leftrightarrow |010\rangle}^{CZ} = \begin{pmatrix} \omega_1 & g_{1c}^{(1)} \\ g_{1c}^{(1)} & \omega_c^{(1)} \end{pmatrix}, \quad (13)$$

$$H_{|101\rangle \leftrightarrow |B_{CZ}\rangle}^{CZ} = \begin{pmatrix} \omega_1 + \omega_2 & g_{1c}^{(1)} \\ g_{1c}^{(1)} & \omega_c^{(1)} + \omega_2 \end{pmatrix}. \quad (14)$$

During the CZ gate, for a prepared state  $|100\rangle$ , the computational states are  $|100\rangle$  and  $|101\rangle$ . The dominant leakage channel appears within the near resonant energy exchange between state  $|100\rangle$  and non-computational state  $|010\rangle$ , and the state leakage dynamic resembles the off-resonant Rabi oscillation which can be described by the two-level Hamiltonian  $H_{|100\rangle \leftrightarrow |010\rangle}^{CZ}$  in Eq.(13)[1, 16]. The periodic oscillation of  $P_{|010\rangle}$  in Fig. 5(b) describes the leakage probabilities to the state  $|010\rangle$  during the CZ gate, which can be suppressed by tuning the wave shape of microwave pulses.

If the initially prepared state is  $|101\rangle$ , where the dominant leakage states appear within the non-computational states  $|011\rangle$  and  $|200\rangle$ , and the leakage dynamics is described by the Hamiltonian of the three-level system[16]. To simplify the dynamic process, the bright mode hybridization  $|B_{CZ}\rangle = \cos(\vartheta)|011\rangle + \sin(\vartheta)|200\rangle$  and dark mode hybridization  $|D\rangle = \sin(\vartheta)|011\rangle + \cos(\vartheta)|200\rangle$  can be introduced, with  $\tan \vartheta = \sqrt{2}g_{12}/g_{1c}^{(1)}$ . In the case of  $g_{1c}^{(1)} \gg g_{12}$ , we have  $\vartheta \approx 0$ , the dark mode is decoupled from states  $|101\rangle$  and  $|B_{CZ}\rangle$ , the bright mode  $|B_{CZ}\rangle$  reduces to  $|011\rangle$  with a transition frequency  $\omega_B = \omega_c^{(1)} + \omega_2$ , and the coupling strength between states  $|101\rangle$  and  $|B_{CZ}\rangle$  is approximately equal to  $g_{1c}^{(1)}$ .

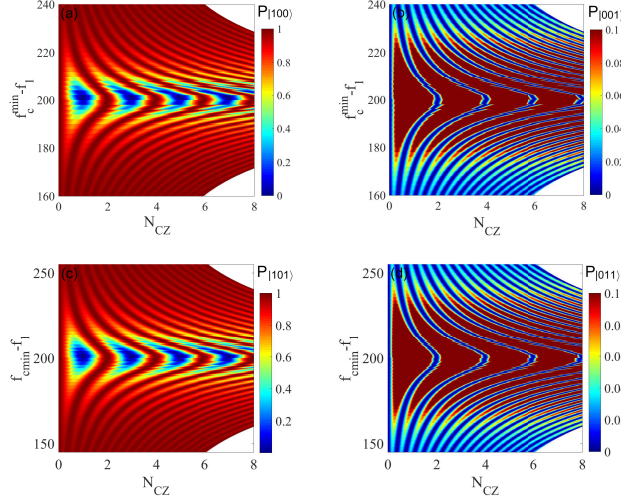


FIG. 5. (Color online) State leakage to the resonator coupler during CZ gate. Populations of states (a)  $|100\rangle$ , (b)  $|010\rangle$ , (c)  $|101\rangle$ , and (d)  $|011\rangle$  changing with the pulse amplitude and CZ gate number  $N_{CZ}$ . The prepared state is  $|100\rangle$  for (a) and (b), but  $|101\rangle$  for (c) and (d). The parameters of the resonator coupler are the same as in Fig. 3(b).

Then the leakage dynamic process can be described by a reduced two-level Hamiltonian  $H_{|101\rangle \leftrightarrow |B_{CZ}\rangle}^{CZ}$  in Eq.(14) and the leakage probabilities  $P_{|B_{CZ}\rangle}$  to bright mode  $|B_{CZ}\rangle$  are described by the periodic oscillation in Fig. 5(d).

## V. CONCLUSIONS

In conclusion, we have proposed a tunable coupler scheme for superconducting Xmon qubits based on a T-shape quarter-wave resonator. In experimentally accessible parameter regime, we studied the effective qubit-qubit coupling, residual ZZ crosstalk, and state leakages. Our tunable coupler scheme is easy for the nano-fabrication and measurement, and less magnetic flux noises will be created to the Xmon qubits. The main limitation for our scheme is to keep the resonator coupler with a relative high quality factor during the frequency tuning by the external magnetic flux. The open ends of the T-shape quarter-wave resonator could help to suppress the ZZ crosstalk and realize high fidelity quantum gates.

## VI. ACKNOWLEDGMENTS

H. W. thanks valuable suggestions from Xiu Gu and Yarui Zheng, and support from Inspur Academy of science and technology. Y.J.Z. is supported by Beijing Natural Science Foundation under Grant No. 4222064 and National Natural Science Foundation of China under Grant No. 11904013. X.-W.X. is supported by the National Natural Science Foundation of China under Grant No. 12064010, and Natural Science Foundation of Hunan Province of China under Grant No. 2021JJ20036.

- 
- [1] Y. Chen, C. Neill, P. Roushan, N. Leung, M. Fang, R. Barends, J. Kelly, B. Campbell, Z. Chen, B. Chiaro, A. Dunsworth, E. Jeffrey, A. Megrant, J. Y. Mutus, P. J. J. ÓMalley, C. M. Quintana, D. Sank, A. Vainsencher, J. Wenner, T. C. White, Michael R. Geller, A. N. Cleland, and J. M. Martinis, qubit Architecture with High Coherence and Fast Tunable Coupling, *Phys. Rev. Lett.* **113**, 220502 (2014).
  - [2] F. Yan, P. Krantz, Y. Sung, M. Kjaergaard, D. L. Campbell, T. P. Orlando, S. Gustavsson, and W. D. Oliver, Tunable Coupling Scheme for Implementing High-Fidelity Two-qubit Gates, *Phys. Rev. Applied* **10**, 054062 (2018).
  - [3] X. Li, T. Cai, H. Yan, Z. Wang, X. Pan, Y. Ma, W. Cai, J. Han, Z. Hua, X. Han, Y. Wu, H. Zhang, H. Wang, Yipu Song, Luming Duan, and Luyan Sun, Tunable Coupler for Realizing a Controlled-Phase Gate with Dynamically Decoupled Regime in a Superconducting Circuit, *Phys. Rev. Applied* **14**, 024070 (2020).

- [4] M. S. Allman, F. Altomare, J. D. Whittaker, K. Cicak, D. Li, A. Sirois, J. Strong, J. D. Teufel, and R. W. Simmonds, rf-SQUID-Mediated Coherent Tunable Coupling between a Superconducting Phase qubit and a Lumped-Element Resonator, *Phys. Rev. Lett.* **104**, 177004 (2010).
- [5] Ming Gong, Shiyu Wang, Chen Zha, Ming-Cheng Chen, He-Liang Huang, Yulin Wu, Qingling Zhu, Youwei Zhao, Shaowei Li, Shaojun Guo, Haoran Qian, Yangsen Ye, Fusheng Chen, Chong Ying, Jiale Yu, Daojin Fan, Dachao Wu, Hong Su, Hui Deng, Hao Rong, Kaili Zhang, Sirui Cao, Jin Lin, Yu Xu, Lihua Sun, Cheng Guo, Na Li, Futian Liang, V. M. Bastidas, Kae Nemoto, W. J. Munro, Yong-Heng Huo, Chao-Yang Lu, Cheng-Zhi Peng, Xiaobo Zhu, Jian-Wei Pan, Quantum walks on a programmable two-dimensional 62-qubit superconducting processor, *Science* **372**, 948 (2021).
- [6] IBM-Q-Team, IBM-Q-53 Rochester backend specification v1.2.0, 2020.
- [7] A. Kandala, K. X. Wei, S. Srinivasan, E. Magesan, S. Carnevale, G. A. Keefe, D. Klaus, O. Dial, and D. C. McKay, Demonstration of a High-Fidelity cnot Gate for Fixed-Frequency Transmons with Engineered ZZ Suppression, *Phys. Rev. Lett.* **127**, 130501 (2021).
- [8] E. A. Sete, A. Q. Chen, R. Manenti, S. Kulshreshtha, and S. Poletto, Floating Tunable Coupler for Scalable Quantum Computing Architectures, *Phys. Rev. Applied* **15**, 064063 (2021).
- [9] Yulin Wu, Wan-Su Bao, Sirui Cao, Fusheng Chen, Ming-Cheng Chen, Xiawei Chen, Tung-Hsun Chung, Hui Deng, Yajie Du, Daojin Fan, Ming Gong, Cheng Guo, Chu Guo, Shaojun Guo, Lianchen Han, Linyin Hong, He-Liang Huang, Yong-Heng Huo, Liping Li, Na Li, Shaowei Li, Yuan Li, Futian Liang, Chun Lin, Jin Lin, Haoran Qian, Dan Qiao, Hao Rong, Hong Su, Lihua Sun, Liangyuan Wang, Shiyu Wang, Dachao Wu, Yu Xu, Kai Yan, Weifeng Yang, Yang Yang, Yangsen Ye, Jianghan Yin, Chong Ying, Jiale Yu, Chen Zha, Cha Zhang, Haibin Zhang, Kaili Zhang, Yiming Zhang, Han Zhao, Youwei Zhao, Liang Zhou, Qingling Zhu, Chao-Yang Lu, Cheng-Zhi Peng, Xiaobo Zhu, and Jian-Wei Pan, Strong Quantum Computational Advantage Using a Superconducting Quantum Processor, *Phys. Rev. Lett.* **127**, 180501 (2021).
- [10] F. Arute, K. Arya, R. Babbush, D. Bacon, J. C. Bardin, R. Barends, R. Biswas, S. Boixo, F. G. S. L. Brandao, D. A. Buell, B. Burkett, Yu Chen, Zijun Chen, B. Chiaro, R. Collins, W. Courtney, A. Dunsworth, E. Farhi, B. Foxen, A. Fowler, C. Gidney, M. Giustina, R. Graff, K. Guerin, S. Habegger, M. P. Harrigan, M. J. Hartmann, A. Ho, M. Hoffmann, T. Huang, T. S. Humble, S. V. Isakov, E. Jeffrey, Zhang Jiang, D. Kafri, K. Kechedzhi, Julian Kelly, P. V. Klimov, S. Knysh, A. Korotkov, F. Kostritsa, D. Landhuis, M. Lindmark, E. Lucero, D. Lyakh, S. Mandrà, J. R. McClean, M. McEwen, A. Megrant, Xiao Mi, K. Michielsen, M. Mohseni, J. Mutus, O. Naaman, M. Neeley, C. Neill, M. Y. Niu, E. Ostby, A. Petukhov, J. C. Platt, C. Quintana, E. G. Rieffel, P. Roushan, N. C. Rubin, D. Sank, K. J. Satzinger, V. Smelyanskiy, K. J. Sung, M. D. Trevithick, A. Vainsencher, B. Villalonga, T. White, Z. J. Yao, P. Yeh, A. Zalcman, H. Neven, J. M. Martinis, Quantum supremacy using a programmable superconducting processor, *Nature* **574**, 505 (2019).
- [11] N. Friis, O. Marty, C. Maier, C. Hempel, M. Holzäpfel, P. Jurcevic, M. B. Plenio, M. Huber, C. Roos, R. Blatt, and B. Lanyon, Observation of Entangled States of a Fully Controlled 20-qubit System, *Phys. Rev. X* **8**, 021012 (2018).
- [12] G.J. Mooney, G. A. L. White, C. D. Hill, and L. C. L. Hollenberg, Whole-device entanglement in a 65-qubit superconducting quantum computer, *arXiv:2102.11521* (2021).
- [13] Xu Zhang, Wenjie Jiang, Jinfeng Deng, Ke Wang, Jiachen Chen, Pengfei Zhang, Wenhui Ren, Hang Dong, Shibo Xu, Yu Gao, Feitong Jin, Xuhao Zhu, Qiujiang Guo, Hekang Li, Chao Song, Zhen Wang, Dong-Ling Deng, H. Wang, Observation of a symmetry-protected topological time crystal with superconducting qubits, <https://arxiv.org/abs/2109.05577>.
- [14] P. Zhao, D. Lan, P. Xu, G.M. Xue, M. Blank, X.S. Tan, H.F. Yu, and Y. Yu, Suppression of Static ZZ Interaction in an All-Transmon Quantum Processor, *Phys. Rev. Applied* **16**, 024037 (2021).
- [15] Y. Xu, J. Chu, J. Yuan, J. Qiu, Y. Zhou, L. Zhang, X. Tan, Y. Yu, S. Liu, J. Li, F. Yan, and D. Yu, Highfidelity, high-scalability two-qubit gate scheme for superconducting qubits, *Phys. Rev. Lett.* **125**, 240503 (2020).
- [16] Y. Sung, L. Ding, J. Braumüller, A. Vepsäläinen, B. Kannan, M. Kjaergaard, A. Greene, G. O. Samach, C. McNally, D. Kim, A. Melville, B. M. Niedzielski, M. E. Schwartz, J. L. Yoder, T. P. Orlando, S. Gustavsson, and W. D. Oliver, Realization of High-Fidelity CZ and ZZ-Free ISWAP Gates with a Tunable Coupler, *Phys. Rev. X* **11**, 021058 (2021).
- [17] P. Mundada, Gengyan Zhang, T. Hazard, and A. Houck, Suppression of qubit Crosstalk in a Tunable Coupling Superconducting Circuit, *Phys. Rev. Applied* **12**, 054023 (2019).
- [18] R. Barends, C. M. Quintana, A. G. Petukhov, Yu Chen, D. Kafri, K. Kechedzhi, R. Collins, O. Naaman, S. Boixo, F. Arute, K. Arya, D. Buell, B. Burkett, Z. Chen, B. Chiaro, A. Dunsworth, B. Foxen, A. Fowler, C. Gidney, M. Giustina, R. Graff, T. Huang, E. Jeffrey, J. Kelly, P. V. Klimov, F. Kostritsa, D. Landhuis, E. Lucero, M. McEwen, A. Megrant, X. Mi, J. Mutus, M. Neeley, C. Neill, E. Ostby, P. Roushan, D. Sank, K. J. Satzinger, A. Vainsencher, T. White, J. Yao, P. Yeh, A. Zalcman, H. Neven, V. N. Smelyanskiy, J. M. Martinis, Diabatic Gates for Frequency-Tunable Superconducting qubits, *Phys. Rev. Lett.* **123**, 210501 (2019).
- [19] Z. L. Wang, Y. P. Zhong, L.J. He, H. Wang, J. M. Martinis, A. N. Cleland, and Q. W. Xie, Quantum state characterization of a fast tunable superconducting resonator, *Appl. Phys. Lett.* **102**, 163503 (2013).
- [20] M. Sandberg, C. M. Wilson, F. Persson, T. Bauch, G. Johansson, V. Shumeiko, T. Duty, and P. Delsing, Tuning the field in a microwave resonator faster than the photon lifetime, *Appl. Phys. Lett.* **92**, 203501 (2008).
- [21] T. Yamaji, S. Kagami, A. Yamaguchi, T. Satoh, K. Koshino, H. Goto, Z. R. Lin, Y. Nakamura, and T. Yamamoto, Spectroscopic observation of the crossover from a classical Duffing oscillator to a Kerr parametric oscillator, *Phys. Rev. A* **105**, 023519 (2022).
- [22] W. Wustmann and V. Shumeiko, Parametric resonance in tunable superconducting cavities, *Phys. Rev. B* **87**, 184501, (2013).
- [23] F.C. Lombardo, F.D. Mazzitelli, A. Soba, and P.I. Villar, Dynamical Casimir effect in a double tunable superconducting circuit, *Phys. Rev. A* **98**, 022512 (2018).

- [24] I.-M. Svensson, Tunable superconducting resonators: Subharmonic oscillations and manipulation of microwaves, Doctoral thesis, Chalmers University of Technology (2018).
- [25] C. Leroux, A. D. Paolo, and A. Blais, Superconducting coupler with exponentially large on-off ratio, *Phys. Rev. Applied* **16**, 064062 (2021).
- [26] J. Koch, T. M. Yu, J. Gambetta, A. A. Houck, D. I. Schuster, J. Majer, A. Blais, M. H. Devoret, S. M. Girvin, and R. J. Schoelkopf, Charge-insensitive qubit design derived from the Cooper pair box, *Phys. Rev. A* **76**, 042319 (2007).
- [27] M. Wallquist, V. S. Shumeiko, and G. Wendin, Selective coupling of superconducting charge qubits mediated by a tunable stripline cavity, *Phys. Rev. B* **74**, 224506 (2006).
- [28] R. Krishnan and J. A. Pople, Approximate fourth-order perturbation theory of the electron correlation energy, *International Journal of Quantum Chemistry* **14**, 91 (1978).
- [29] Guanyu Zhu, D. G. Ferguson, V. E. Manucharyan, and J. Koch, Circuit QED with fluxonium qubits: Theory of the dispersive regime, *Phys. Rev. B* **87**, 024510 (2013).